Proceedings of IMECE'03
2003 ASME International Mechanical Engineering Congress
Washington, D.C., November 15–21, 2003

IMECE2003-55554

DESIGN OF HIGH PRECISION HIGH BANDWIDTH AND RELIABLE NANOPOSITIONING SYSTEMS

Srinivasa Salapaka
Laboratory for Information and Decision Systems
Massachusetts Institute of Technology, MA 02139
Email: svasu@mit.edu

Abu Sebastian
Department of Electrical and Computer Engineering
Iowa State University, Ames, IA 50011
Email:abuseb@iastate.edu

ABSTRACT

In this paper, we present a paradigm which prescribes a procedure for a systematic design, analysis and development of nanopositioning devices. In this effort, we have used many tools from modern control theory to model devices, to quantify device resolution, bandwidth, range, and robustness, and to tackle undesirable nonlinear effects such as hysteresis and creep. The implementation of this procedure for the simultaneous *achievement of robustness, high precision, and high bandwidth objectives is presented. The merits of the paradigm are demonstrated through experimental results.*

Introduction

The invention of scanning probe microscopes such as Atomic Force Microscopes (AFM) [1] has revolutionized research by making it possible to investigate matter at atomic scales. Recent demonstrations using these microcantilever based devices and the ensuing research in this direction in the last decade [2, 3] provide ample evidence to the feasibility of *nanotechnology* - i.e. rational control, manipulation and interrogation of matter at atomic scales. This technology includes applications in precision engineering and electronics [3–5], electromechanical systems (e.g. 'lab on a chip' devices) as well as mainstream biomedical applications in areas as diverse as gene therapy, drug delivery and drug discovery techniques. It has been predicted that its impact on the health, wealth and the lives of people will be at least equivalent to the combined influences of microelectronics, medical imaging, computer aided engineering and man made polymers developed in the last century.

One of the pivotal requirements of nanotechnology is nanopositioning. The interrogation and manipulation at atomic scales demands positioning systems with atomic scale resolutions. For example nanopositioning systems are necessary in scanning probe microscopy to provide subnanometer-resolution motions in order to probe molecular and atomic features on a sample, in test equipments for semiconductors such as mask and wafer inspection systems [6], in grading and testing disk drive read-write heads [7], in characterizing magnetic media and recording methods, in optical alignment systems [8, 9], in molecular biology [10, 11], and in synchotrons for X-ray microscopy.

Typically, the nanopositioning devices are actuated by piezoelectric materials. The crystal lattices of these materials deform on application of an electric field. These deformations are used for accurate positioning. The advantages of these actuators are several: they provide repeatable sub-nanometer motion, do not have backlash, do not suffer from wear and tear, require very little maintenance, have fast response times, can generate large forces, are operable in a wide range of temperatures, and are not affected by magnetic fields. However, their use is hindered by nonlinear effects like hysteresis and creep. Hysteretic effects, in which the piezo motion does not vary linearly with the applied voltage are prominent especially in large traversals and can be as high as 10-15% of the path covered. Creep, in which the piezo drifts independent of the applied voltage, becomes noticeable when positioning is required over long time periods.

In this paper, we present the importance of modern control theoretic tools in addressing these demands and challenges on the nanopositioning systems. The compensation of the hysteretic and creep effects form only a small portion of the demands

on the design. The main design challenges come from the demands on the bandwidth, precision and robustness. We show how many of the popular approaches in the nanopositioning industry are inadequate in obtaining simultaneously these objectives while the modern control approach, in contrast, provides an apt paradigm to incorporate these objectives, obtain models of these devices, to quantify device in terms of resolution, bandwidth, range and sensitivity, and tackle hysteresis and creep. In particular, we present the $\mathcal{H}_\infty$ control designs (nominal, robust and Glover-McFarlane) and contrast it with the more prevalent proportional integral (PI) and proportional double integral (PII) designs. We demonstrate this approach through a design of a nanopositioning system. Our contributions in this paper are two fold: (1) identification of demands and challenges in nanopositioning systems and their translation to the control paradigm, and (2) application of this paradigm in designing, building and characterizing nanopositioning devices with a special emphasis on the bandwidth, resolution and robustness.

The paper is organized as follows: in section 1 we identify the requirements on the design of nanopositioning devices and present some of the approaches popular in nanopositioning industry in meeting them. In section 2, we describe the essential features of a nanopositioning device and associated challenges. In section 3, we present two nanopositioning devices with these features and demonstrate the importance and advantages of the modern control theory tools in their design and characterization. In section 4, we present some observations and future directions.

1 Requirements and Current Approaches

In this section we list the typical requirements on nanopositioning devices. The requirements on these devices are primarily of high precision, high bandwidth and robustness. In many nanotechnological applications and nanoscientific experiments, positioning accuracies in angstroms are typically specified. For example in scanning probe microscopy molecular and atomic forces are routinely probed which require subnanometer resolution positioning capabilities. In many studies, it is critical that the probe is positioned exactly (within atomic tolerances), since inaccuracy in this positioning can make the study invalid. Another important demand on performance of these devices is the bandwidth. Since the applications (such as nano-imaging) require to investigate (manipulate or control) matter with subnanometer resolutions of areas which are two orders or higher ($5\ \mu m$ scans are common), it becomes important to have fast positioning devices (open loop systems have bandwidths in order of $5\ Hz$ while requirements can be two to four orders higher). Furthermore, in some applications high bandwidth positioning is necessary. For instance, some biological studies of cell dynamics *require* micro/nano second imaging capabilities. Besides these demands on performance, it is also very important for the devices to be reliable - i.e. robust to the changing environments. Typically, these devices are found to be sensitive to the uncertainties in the environment and operating points. This sensitivity, if not accounted for can result in unreliable and spurious experimental data. Also since these devices are used by diverse users in multitude of environments, it cannot be expected of them to have the technological know how to tune the device to the appropriate operating point. Therefore robustness to modelling and environment uncertainties is crucial for these devices.

In nanopositioning industry, these devices are typically designed for open loop operation. The data is then post processed to account for the hysteretic and creep effects [12]. In this mode of operation, the device motions are restricted to set of specific repetitive trajectories where the non linear effects can be effectively compensated. This becomes unacceptable for some applications where tracking of non standard trajectories is needed (for example in nanolithography). This method also needs extensive characterization of the device since the design of precompensated input signals is very sensitive to inaccuracies in modelling. Moreover, this method also demands very high quality actuators (as there is no real time corrective mechanism) which makes the device very expensive.

There have been many efforts to counter the nonlinear effects which include design changes in the open-loop implementation such as: using 'harder' piezoceramics which have smaller nonlinear effects at the cost of travel range (see Ref. [13]); replacing voltage control by charge control (see Ref. [14]) which achieves lower hysteresis but leads to more creep, lesser travel and lower positioning bandwidth; and compensating for the adverse nonlinear effects by a careful modelling of the nonlinearities which achieves good results but is sensitive to the precision of the model used (see Ref. [15]).

In comparison to the open loop architecture there are fewer feedback design schemes for nanopositioning. The feedback laws, when employed in nanopositioning industry, are usually Proportional Integral (PI) or Proportional double integral (PII) control laws. These laws provide high gains at low frequencies and greatly diminish the hysteretic and creep effects. However, they achieve very low bandwidths and have poor robustness properties. This low bandwidth can be explained from the following simplified analysis. The transfer functions representing the nanopositioning systems usually have very low damping values for the slowest modes. So, if we approximate the system by considering only its slow modes $x \pm iy$, the PI control law results in a third order closed loop system where the characteristic polynomial is given by $s^3 + 2\delta\omega_n s^2 + (k_p + w_n^2)s + k_i$, where $\omega_n \stackrel{\triangle}{=} \sqrt{(x^2+y^2)}$ and $\delta \stackrel{\triangle}{=} x/\omega_n$. For this system the bandwidth is in the order of $\delta\omega_n$. For the devices that we studied ω_n was approximately 400 Hz and the damping δ was around 0.008 which gives an estimate of 3.2 Hz on the bandwidth. The PII designs are used to achieve asymptotic tracking of ramp signals which are important for imaging applications. These design fails

to achieve high bandwidths. Another disadvantage of using these designs for these systems is that the resulting closed loop systems have poor robustness properties. This will be demonstrated in detail in Section 3. Proportional-Integral-Derivative (PID) and Proportional-double-Integral-Derivative (PIID) designs do provide more design parameters than the PI and PII designs respectively. However, they are avoided in the industry as derivative term amplifies the resolution degradation problem. These design laws along with other classical loop shaping methods aim at addressing specific challenges and it is substantially difficult to tackling all the challenges simultaneously. Especially it requires a considerable amount of expertise in tuning these parameters and obtain a good trade-off (which might not even be possible in designs such as PI) between the resolution and bandwidth while keeping the closed loop system robust to uncertainties in model and environment. On the other hand, modern control theory provides an apt paradigm to incorporate all the demands and design feedback laws to achieve them. The use of control methodologies for these systems have been few: In Ref. [16], the design of a feedback controller using an optical sensor attachment to enhance the performance of an Atomic Force Microscope scanner is described. Similar efforts to improve the scanning speeds of the AFM are made in Ref. [17]. In this paper, we demonstrate this through the control designs of devices that we have developed by reviewing some of the designs presented in [18] and [19] and present some new control designs.

2 Essential Elements and Challenges

We have identified three elements in nanopositioning devices which are essential to achieve *simultaneously* the demands of high precision, high bandwidth and robustness.

Flexure stages form a basic element. They provide motions by elastic deformations and therefore do not suffer from effects such as backlash. As a consequence, these deformations provide repeatable motions with atomic scale resolutions and are in fact limited only by thermal noise. Thus they serve as reliable platforms for placing and positioning samples for atomic scale investigations. Moreover the force-displacement curves are linear which makes their use simple. Also, they are easy to fabricate (by electron discharge machining) and give reliable motions in a multitude of environments and operating conditions. However, these stages lead to limitations in achievable bandwidth on account of the 'flexure dynamics' that is introduced. Since the actuators and sensors are connected by a flexure stage, the motion imparted by the actuation is not necessarily transmitted to the point of intended operation or detection (and in fact, there can be an inverse input-output response). The transfer functions describing these systems are non minimum phase (have zeros in the right half plane) which pose a limitation on achievable bandwidths. Another drawback is that these devices can have out-of-plane motions (can move in z direction when actuated in $x-y$ plane) which can pose a difficulty in probing the samples.

Piezoactuators form another basic element. They provide motion (and actuation force) by the piezoelectric property in which a piezoelectric crystal deforms on application of electric field. These deformations provide motions with angstrom scale resolutions and provide large forces to move the flexure stages. They do not suffer from effects as backlash as there are no sliding parts. They are very robust devices and can be used in a large range of temperatures and operating conditions. However, they input voltage-deformation relationships are not linear but show hysteresis. The hysteretic effects can be as big as 10% which poses a challenge for repeatable and reliable positioning. Also, they suffer from creep phenomenon in which they move due to remnant polarization even when a constant input voltage is applied. Another limitation of piezoactuation is that control signals have to be within its saturation limits (for instance stack piezos are restricted to have only negative inputs up to about $-10\ V$ as they get depoled when positive inputs are given).

Feedback control design is another basic element for these devices. It is essential in *simultaneously* achieving the bandwidth, resolution and robustness requirements. This makes it necessary to have high resolution sensors for feedback, high bandwidth-high resolution data acquisition components to collect the sensor data and fast digital signal processors to implement the feedback algorithms. The main challenge comes from the feedback itself. The feedback of noisy sensor data degrades the device resolution. This is an important issue since achieving high resolution forms one of the main objectives. However, feedback is essential to tackle hysteretic and creep effects, and more importantly, to achieve high bandwidths and robustness. This puts an added emphasis on designing appropriate feedback laws to play this trade-off between achieving high bandwidth and maintaining high resolution. The robustness requirements pose difficult challenges to design. The frequency responses typically show a wide variation with operating points and even show time varying pole shifts at the same operating point. The *simultaneous* fulfilment of these demands on the design coming from the requirements on performance and robustness, and from the constraints on the actuator poses the largest challenge on the feedback design.

3 Nanopositioning Devices

Here, we present two devices that have the elements described in the previous section. We first present the device which is capable of positioning in one dimension. For this device, we present and compare the PI and the nominal $\mathcal{H}_\infty$ designs. Here the control design for this device was primarily done to achieve high bandwidth and resolution especially since the non-collocated actuator/sensor effects were significant and the transfer function representing system had a pair of non minimum phase zeros. The $\mathcal{H}_\infty$ controller achieved good robustness mar-

gins. Then we present another device which is a two dimensional positioning device. For this device we present the PII, Robust $\mathcal{H}_\infty$ and Glover McFarlane designs. Here the aim was to achieve objectives of resolution and bandwidth while guaranteeing robustness. The robustness requirements formed an important challenge in this device since the frequency responses showed time varying pole shifts in addition to the variation with operating points. These requirements along with the bandwidth and resolution demands were included in the control design. Especially, in the Glover McFarlane design, these requirements fall naturally in its framework, where performance and robustness objectives are simultaneously achieved.

3.1 One dimensional nanopositioning device

The nanopositioning system studied in this paper is described in Figure 1 (developed in *Asylum Research*, Santa Barbara, California). The main idea is based on the elastic deformation of the flexure stage which is used for nanopositioning. This motion is obtained by the serpentine spring design (see Figure 1) where design grooves (about $150\mu m$ wide) are cut in the base plate, making it possible for the central block containing the sample to move relative to the frame.

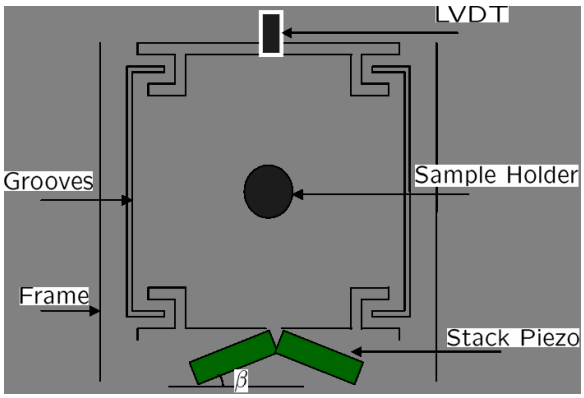

Figure 1. A SCHEMATIC OF THE NANOPOSITIONING DEVICE. THE FLEXURE STAGE PROVIDES MOTION BY VIRTUE OF THE SERPENTINE SPRING DESIGN. THE GROOVES SHOWN IN THE FIGURE ARE EXAGGERATED AND NOT DRAWN TO SCALE. THE STAGE IS ACTUATED BY PIEZO-ELECTRIC STACKS AND THE RESULTING MOTION IS SENSED BY LVDT SENSOR.

The forces to induce elastic deformations are generated by stack-piezos. As shown in Figure 15, these piezo stacks are at an angle $\beta \approx 7.5$ degrees which gives a mechanical gain of $1/\sin(\beta)$. The motion of the flexure stage is measured by the LVDT (Linear Variable Differential Transformer) and the associated demodulation circuit.

The flexure based design has no sliding parts which rules out effects such as backlash. As a result motions with atomic scale resolutions can be obtained. Besides being cheaper, the piezostacks have longer travel ranges compared to their cylindrical counterparts used in commercial AFMs. These actuators lead to a travel range of approximately $75\mu m$. The modified LVDT sensors used in this design have resolution in the order of 2 Å over a 1 *kHz* bandwidth which gives a vast advantage over more common optical sensors. However, open-loop operation of piezostacks suffers from relatively large effects of hysteresis and creep. This places an added importance to the control system. In this device, the control laws are implemented on a *Texas Instruments C44* digital signal processor.

In this paper, we denote the input to the actuation system by u, the demodulated output signal from the LVDT by y and the system comprising the actuation, flexure and detection stages by G. Also, we refer to u as the piezo-input, y as the LVDT-output and G as the plant. Figure 2 is a schematic block diagram of

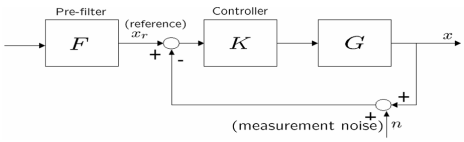

Figure 2. A SCHEMATIC BLOCK DIAGRAM OF THE CLOSED LOOP SYSTEM.

the closed loop system. Here x_r represents the reference or the command signal; e denotes the error signal, the difference between the reference and the output signals; and K stands for the controller transfer function. Also, we represent the sensitivity function, i.e., the transfer function from r to e by S; and the complimentary sensitivity function i.e., the transfer function from r to y by T. The tradeoff between achieving high tracking bandwidth and maintaining high resolution translates to designing K such that S is low in the frequencies of reference signals while at the same time rolling off T to mitigate the effects of sensor noise on resolution.

3.1.1 Identification of the system The transfer function G to describe the device was obtained by obtaining it frequency response about an operating point. The nominal operating point is chosen to be the *null position*, i.e. where the LVDT outputs read zero. This was done using a HP signal analyzer which gave a sine sweep of 50 *mV* signals with frequencies spanning over a bandwidth of 2 *kHz*. The frequency response of the device at this operating point is shown by the Bode plot (dashed lines) in Figure 3. Accordingly, a fourth order non min-

imum phase transfer function:

$$G(s) = \frac{9.7 \times 10^4 (s - (7.2 \pm 7.4i) \times 10^3)}{(s + (1.9 \pm 4.5i) \times 10^3)(s + (1.2 \pm 15.2i) \times 10^2)}$$

was fit to this data. Figure 3 shows that there is a good match between this frequency response data and the one simulated from the model, $G(s)$.

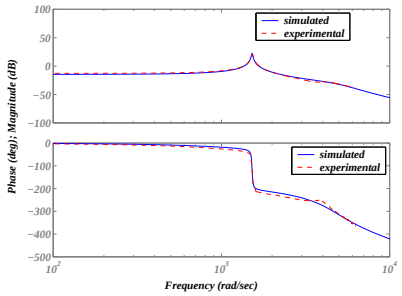

Figure 3. A COMPARISON OF EXPERIMENTALLY OBTAINED AND SIMULATED FREQUENCY RESPONSES OF THE PLANT.

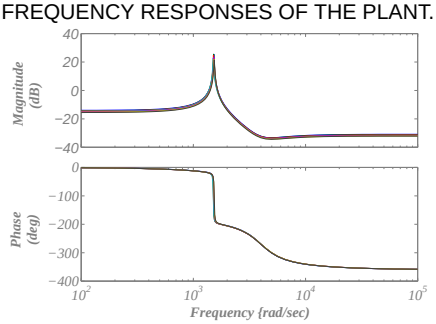

Figure 4. FREQUENCY RESPONSES OF THE PLANT G AT DIFFERENT OPERATING POINTS.

This process was then repeated to identify the system at different operating points (by giving various DC offsets) spanning the range of operation of the device. It was found that the frequency responses agreed with each other at higher frequencies and were different in their DC values (see Figure 4). This motivates the design of controllers which guarantee robustness.

3.1.2 Control Design The feedback laws for this device were implemented primarily to achieve high bandwidths ($\approx 150Hz$) and subnanometer resolution. These laws are constrained to provide control signals that were negative and within actuator saturation limits (-10 V to 0 V). Besides these implementation constraints, the presence of RHP zeros imposes fundamental constraints. For example, from classical root locus analysis we know non minimum phase zeros imply high gain instability of the system. In fact pure gain controllers with gains greater than 0.1674 are ruled out for this system. As discussed in Section 1, they also impose a fundamental limit on the achievable bandwidth of the closed loop system. The achievable ideal bandwidth is approximately 415 Hz for the system. This controller is "ideal" in the sense that it may not be realizable and which, for a unit step reference $r(t)$, generates an input $u(t)$ which minimizes the integral square tracking error $\int_0^\infty |y(t) - r(t)|^2 dt$ [20].

PI **controller design**
Since we know the structure of the controller ($k_p + k_i/s$), we can determine the regions in the k_p-k_i plane which guarantee closed loop stability. Figure 5(a) shows this plot. It should be noted that the region (in the k_p-k_i plane) that gives high bandwidth (see plot (d)) is the region with low gain margin (see plot (c)), i.e. there is a trade-off between robustness and performance. We chose $k_p = 0.01$ and $k_i = 75$, which guarantee a gain margin of 1.57 and a phase margin of 89° and the corresponding bandwidth of the closed loop transfer function is 2.12 Hz. This controller was implemented and Figure 6 shows tracking of a 1 Hz triangular wave. We see that there is an excellent agreement between the reference and the LVDT-output signals for this input.

It should be noted that the bandwidth ($< 3Hz$) attained here is much less than the "ideal" bandwidth (≈ 415 Hz). This low bandwidth agrees well with simplified analysis we presented in Section 1. The main reason for the failure of the PI design is that the poles of the closed loop system (even for the third order system) cannot be placed arbitrarily by choosing k_p and k_i. A higher order controller is needed to have full freedom in the placement of poles. This motivates us to look into more sophisticated designs. We present the design of $\mathcal{H}_\infty$-controller in the next section.

$\mathcal{H}_\infty$ **controller design**
The main advantage of using this design is that it includes the performance objectives in the problem formulation itself. In the system (see Figure 7(b)), the exogenous input w is the reference signal r, the control input is u and the measured output v is the error signal e. In order to reflect the performance objectives and physical constraints, the regulated outputs were chosen to be the weighted transfer function, $z_1 = W_1 e$, the weighted system output, $z_2 = W_2 y$ and the weighted control input, $z_3 = W_3 u$. In this way, the transfer function from w to z_1 is the weighted sensitivity function, $W_1 S$, which characterizes the performance objective of good tracking; the transfer function from w to z_2 is the complementary sensitivity function, whose minimization ensures low control gains at high frequencies, and the transfer function from w to z_3 is KS, which measures the control effort. The weight-

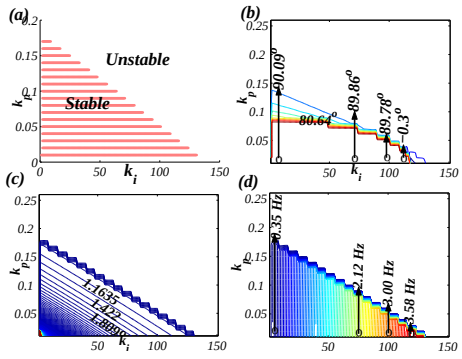

Figure 5. (a) THE REGION IN K_I-K_P PLANE THAT GUARANTEES CLOSED LOOP STABILITY. THE CONTOUR PLOTS SHOWING (b)THE PHASE MARGINS (c) THE GAIN MARGINS (d) THE BANDWIDTHS OF THE CLOSED LOOP SYSTEMS CORRESPONDING TO DIFFERENT POINTS IN THE K_I-K_P PLANE.

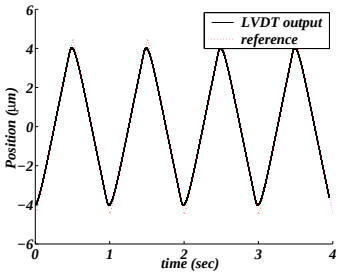

Figure 6. TRACKING OF 1 HZ TRIANGULAR SIGNAL WITH PI CONTROLLER.

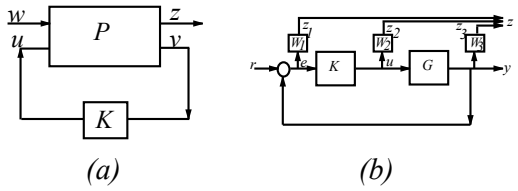

Figure 7. (a) THE GENERALIZED PLANT FRAMEWORK. (b) THE CLOSED LOOP SYSTEM WITH REGULATED OUTPUTS.

ing functions W_i, $i = 1,2$ and 3 are used to scale these closed loop transfer functions to specify the frequency information of the performance objectives and system limitations (see Figure 8). W_1 was chosen to be a first order transfer function,

$$W_1(s) = \frac{0.1667s + 2827}{s + 2.827}.$$

This transfer function is designed so that its inverse (an approximate upper bound on the sensitivity function) has a gain of 0.1% at low frequencies (< 1 Hz) and a gain of $\approx 5\%$ around 200 Hz. We scale the complementary sensitivity function, T, by

$$W_2 = \frac{s + 235.6}{0.01s + 1414}$$

which ensures rolling off of T at high frequencies. The transfer function, KS was scaled by a constant weighting $W_3 = 0.1$, to restrict the magnitude of the input signals such that they are within the saturation limits. This weighting constant gives control signals that are at most six times the reference signals.

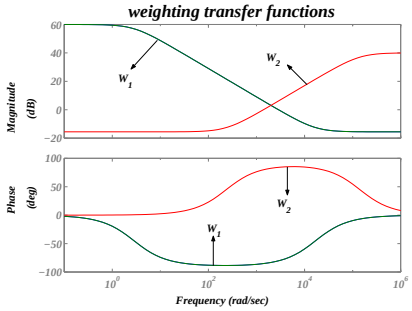

Figure 8. THE WEIGHTING TRANSFER FUNCTIONS.

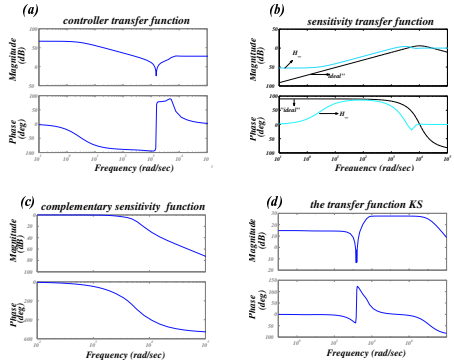

Figure 9. CLOSED LOOP TRANSFER FUNCTIONS: (a)CONTROLLER (b) SENSITIVITY (c) COMPLEMENTARY SENSITIVITY (d)KS

A controller transfer function K such that

$$\left\| \begin{bmatrix} W_1 S \\ W_2 T \\ W_3 KS \end{bmatrix} \right\|_\infty < \gamma$$

where $\gamma = 2.415$ (found iteratively by the control algorithm) was designed using Matlab. The following sixth order controller transfer function, $K(s)$ was obtained with a DC gain of $2.2599 \times$

10^3, its poles at $-1.14959 \times 10^7, -1.4137 \times 10^5, -5.6432 \times 10^3, -2.8274$ and $(-1.5676 \pm 5.8438i) \times 10^3$, and its zeroes at $-1.4137 \times 10^5, (-1.8647 \pm 4.4958i) \times 10^3$ and $-1.1713 \times 10^1 \pm 1.5205i \times 10^3$.

The controller, the sensitivity, the complementary sensitivity function and KS transfer functions are shown in Figure 9. The bandwidth of the system (from the sensitivity transfer function) is found to be 138 Hz. It should be noted that this is an enormous improvement over the PI controller. Also, this controller provides a gain margin of 2.57 and a phase margin of 62.3° as opposed to the values of 1.57 and 89° in the PI controller. In this figure (plot (b)), we have compared the sensitivity function with the"ideal" one introduced earlier in the section.

Figure 10 compares its performance with the PI controller for a 5 Hz triangular wave. It should be noted that the performance of the $\mathcal{H}_\infty$ controller is significantly better than the PI controller. Figure 11 compares the bandwidths obtained by this design. The PI controller achieves a bandwidth of 2.24 Hz while the $\mathcal{H}_\infty$ controller achieves 138.3 Hz - an improvement of over sixty times!

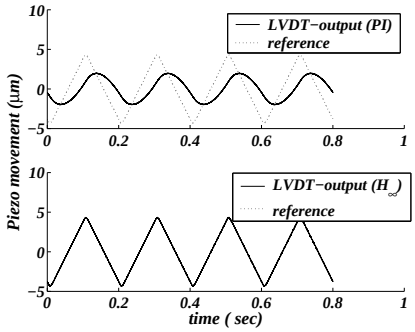

Figure 10. A COMPARISON OF THE PERFORMANCE OF THE CLOSED LOOP SYSTEM WITH (a) PI CONTROLLER (b) $\mathcal{H}_\infty$ CONTROLLER.

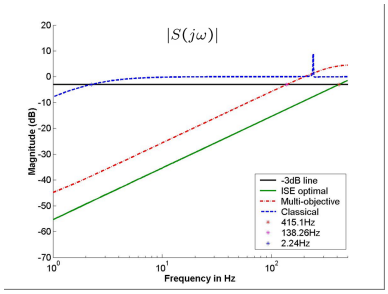

Figure 11. A COMPARISON OF BANDWIDTHS ACHIEVED BY PI, $\mathcal{H}_\infty$ AND "IDEAL" CONTROLLERS.

3.1.3 Elimination of nonlinear effects The positioning precision of the piezoactuators is significantly reduced due to nonlinear effects such as hysteresis, drift and creep. However, with the feedback control laws, these nonlinear effects are compensated and thus the closed loop device does not show any hysteresis. The hysteresis plots were obtained by giving input signals (less than 1 Hz triangular pulses) of increasing amplitudes (1 V to 4 V) and recording the corresponding output signals. Then the output vs reference plots were made (see Figure 12(a)). It is observed that the hysteresis effects are dominant at higher amplitudes (longer travels) and become smaller as the travel lengths are reduced. The maximum output hysteresis varies from 0.74μm to 4.93μm (7.2% to 10% of corresponding travels). A similar plot (see Figure 12(b)) obtained for the closed loop configuration shows that the feedback control laws virtually eliminate all hysteretic effects and the output and reference signals match well. In this case, the travel length is 45μm and the maximum output hysteresis was significantly reduced to 62.3 nm (0.14%) and the corresponding maximum input hysteresis was reduced to 2 mV (0.07%).

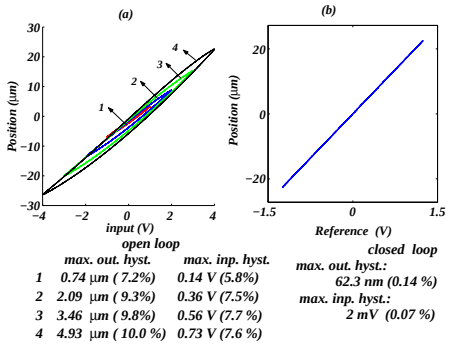

Figure 12. HYSTERESIS IN (a) THE OPEN LOOP CONFIGURATION, (b) ITS ELIMINATION IN THE CLOSED LOOP CONFIGURATION.

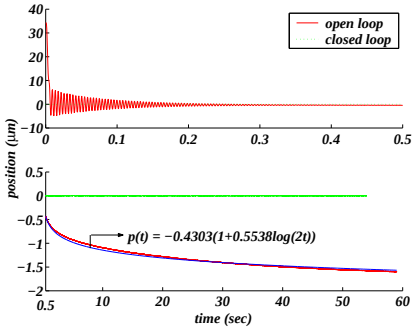

Figure 13. (a) RESPONSES TO THE STEP INPUT OF OPEN LOOP AND CLOSED LOOP SYSTEMS (b) THE ELIMINATION OF CREEP IN THE CLOSED LOOP SYSTEM AND ITS APPROXIMATION BY A CREEP LAW.

The creep effect is approximately described by the equation,

$$y(t) \approx y_0(1+\gamma \log(t/t_0)),$$

where t_0 is the time at which the creep effect is discernible, y_0 is the value of the signal at t_0 and γ is a constant, called the creep factor, that characterizes this nonlinear effect. We see that the output in the open loop case responds to the reference signal (see Figure 13) but instead of reaching a steady state value it continues to decrease at a very slow rate. The response $y(t)$ was found to approximately satisfy the creep law with a creep factor of 0.55 The same experiment conducted in the closed loop shows that the feedback laws virtually eliminate this effect and the system tracks the reference signal exactly.

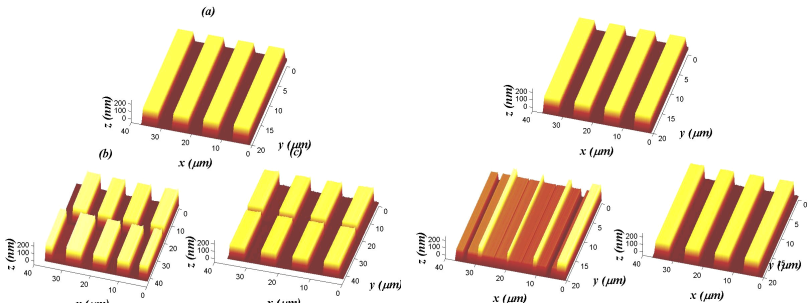

Figure 14. LEFT: (a) THE REFERENCE (CALIBRATION SAMPLE) GEOMETRY. (b) THE MISMATCH IN THE POSITION OF GROOVES BETWEEN THE FORWARD AND THE BACKWARD TRAVERSES IN THE OPEN LOOP. (c) A GOOD MATCH IN THE CLOSED LOOP CONFIGURATION. RIGHT: (a) THE CALIBRATION SAMPLE (TOP) (b) ITS DISTORTED IMAGE OBTAINED BY AVERAGED DATA IN THE OPEN LOOP CONFIGURATION (BOTTOM-LEFT). (c) ITS FAITHFUL IMAGE OBTAINED BY AVERAGING IN THE CLOSED LOOP (BOTTOM-RIGHT).

Repeatability

A significant adverse effect of the nonlinearities in the open loop is that of non repeatability. This was seen clearly in the calibration experiment described in the previous section. In the open loop case, the grooves that were observed when travelling in one direction were not concomitant with those in the other direction. Also, the images were distorted in the open loop scans. These effects were removed with feedback control (the results using the $\mathcal{H}_\infty$ controller is shown here. The scanning speeds were beyond the bandwidth achieved by the PI law). The mismatch in the open loop is more clearly seen in the left plot in Figure 14, where the image obtained in one direction is kept behind the one got in the other direction for the sake of comparison. In (c), the near perfect match with the closed loop system is demonstrated. This non repeatability can lead to gross errors when the images are averaged over many scans (say to remove the effects of noise). For example, the right plot in Figure 14(bottom-left) shows the scan of grooves obtained by averaging over the forward and the backward directions. It can be seen that it has no semblance with the actual calibration sample (top). However, the averaged scan in the closed loop case, (bottom-right), matches very well with the sample.

3.2 Two dimensional nanopositioning device

This device has the same working principle as the device described in the previous section except that it provides motion in two directions. The flexure stage consists of two stages, 'X' seated on 'Y' (see Figure 15), with the sample holder on the 'X' stage.

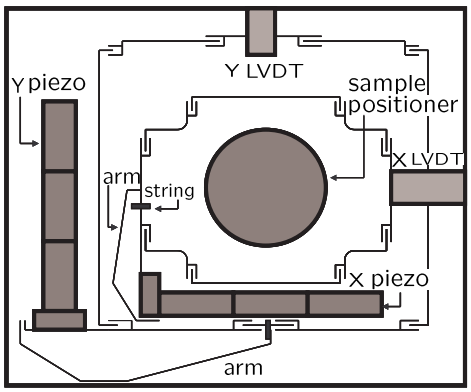

Figure 15. A SCHEMATIC OF THE NANOPOSITIONING DEVICE. THERE ARE TWO STAGES 'X' AND 'Y' WITH 'X' SITTING ON TOP OF 'Y'. EACH STAGE IS ACTUATED BY PIEZO-ELECTRIC STACKS AND THE RESULTING MOTION IS SENSED BY LVDT SENSORS.

Each stage, by virtue of the serpentine spring design deforms under the application of force providing motion. These forces are generated by stack-piezos. As shown in Figure 15, there are three piezo-actuators in series for each axis. The motion of each stage is measured by the respective LVDT (Linear Variable Differential Transformer) and the associated demodulation circuit. In this device, the control laws are implemented on a *Analog Devices ADSP-21160* digital signal processor.

3.2.1 Identification The device is viewed as a two-input two-output system where the low voltage signals to the 'X' and 'Y' amplifiers (u_x and u_y) are the inputs and the motion of 'X' and 'Y' stages measured by the respective LVDT sensors, (x and y) are the outputs. This results in four input-output transfer functions, $G_{ij}, i, j \in \{x, y\}$. Here G_{ij} represents the transfer function from the input u_j to the output i. These maps were identified

using frequency response about the null position. The responses were obtained using a *HP3536A* signal analyzer with 10 mV amplitude forcing and averaged over 200 measurements for a bandwidth of 1.25kHz. $G_{xx}(s)$, a 7th order transfer function with the first resonance frequency at approximately 390 Hz, was fit to the frequency response. $G_{yy}(s)$ is 5th order with the first resonance frequency at 235 Hz. The coupling transfer functions G_{xy} and G_{yx} are negligible compared to the diagonal transfer functions and therefore were neglected in order to simplify the design process. The mode of operation of this device is such that higher bandwidth requirements are made on the smaller stage 'X' where as 'Y' stage is made to move relatively slow. Hence, there is a greater emphasis on the control designs for the 'X' stage which is presented in this paper. Designs were also done for G_{yy} and the resulting diagonal controllers were implemented, the details of which are not presented in this paper. The transfer function G_{xx} is given by

$$G_{xx}(s) = \frac{4.29\times10^{10}(s^2+631.2s+9.4\times10^6)(s^2+638.8s+4.5\times10^7)}{(s^2+178.2s+6\times10^6)(s^2+412.3s+1.6\times10^7)(s^2+209.7s+5.6\times10^7)(s+5818)},$$

and its fit to the experimental data is shown in Figure 16 In

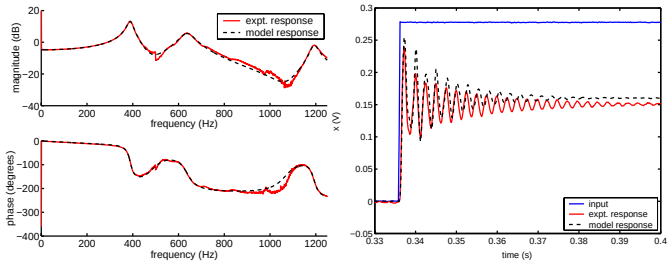

Figure 16. LEFT: EXPERIMENTAL FREQUENCY RESPONSE IS COMPARED WITH THE RESPONSE OF THE MODEL $G_{XX}(S)$. RIGHT: THE EXPERIMENTAL STEP RESPONSE IS COMPARED WITH THE RESPONSE OF G_{XX}.

order to further validate the models, step responses obtained experimentally are compared with the model responses. In Figure 16 (right plot), a comparison of the step responses shows agreement between the two responses for both G_{xx}. The slight variation in gain could be attributed to hysteresis since the models are obtained using low amplitude (10 mV) signals whereas the step response in this experiment has a magnitude of around 200 mV.

To study the variation of these models to the operating points, frequency responses are obtained at different operating points. A considerable variation was observed in these responses. Figure 17 shows the responses obtained at different operating points spread over a range of approximately 80 μm, separated by approximately 20 μm. Further it was observed that the frequency response at the same operating point varies when obtained at different times. These uncertainties in the model make robustness

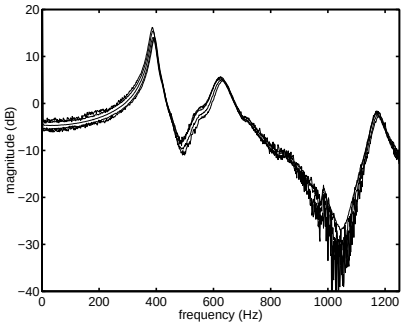

Figure 17. EXPERIMENTALLY OBTAINED FREQUENCY RESPONSES AT DIFFERENT OPERATING REGIONS FOR THE X STAGE.

of the closed loop system a key requirement. The design of the feedback laws to achieve these requirements is presented in the next section.

3.2.2 Control Design The control design for the one dimensional device was primarily done to achieve performance bandwidths. Here the robustness becomes an important issue. The pole shifts in the model are not accounted for by the nominal $\mathcal{H}_\infty$ design. Here we present the robust $\mathcal{H}_\infty$ and the Glover McFarlane designs which we implemented and compare these designs to the PII designs in the industry.

Proportional double integral (PII) control design
These designs are popular as they are simple to implement. Moreover an attractive feature of these controllers is that they can track ramp signals (common in imaging applications) with zero steady state errors. Here a PII design is presented which has been obtained after considerable search and tuning over the parameter space. It is given by $K_{pii}(s) = \frac{0.001s^2+450s+10^5}{s^2}$. This controller was implemented and the experimental bode plot of S is shown in Figure 18. Besides having a low closed loop bandwidth of 37 Hz, this design has poor robustness properties. The tracking of signals with frequencies as low as 5 Hz is unsatisfactory. The shows that the usable region of the trajectory is only 30% of the total period. The $\|S\|_\infty$ for K_{pii} is 13.8 dB which results in lower bounds on GM and PM of 1.25 and 11.73 degrees respectively. Due to the low phase margin, attempts to introduce a low pass filter within the loop to improve the resolution results in instability.

$\mathcal{H}_\infty$ control design
A nominal $\mathcal{H}_\infty$ design was done for this system on the same lines

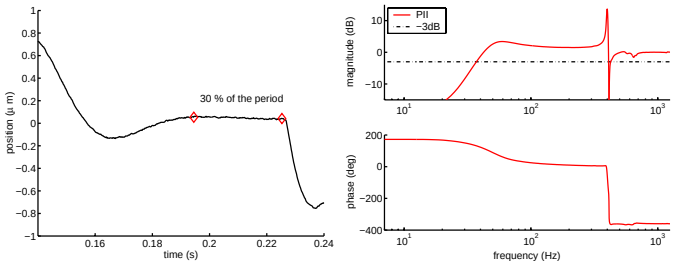

Figure 18. LEFT: AT 5 HZ, OSCILLATORY BEHAVIOR IS OBSERVED WHICH REDUCES THE REGION OF THE TRAJECTORY WHICH CAN BE USED FOR SCANNING PURPOSES. RIGHT: THE EXPERIMENTAL BODE PLOT OF THE SENSITIVITY FUNCTION IS SHOWN FOR A PII CONTROLLER. THE PEAKS IN THE MAGNITUDE PLOT INDICATE LACK OF ROBUSTNESS.

as done for the one dimensional device. The controller was found to be non-robust and was found to have poor noise characteristics after implementation. The reason for this behavior is that the nominal $\mathcal{H}_\infty$ design does not account for pole uncertainties which are crucial for G_{xx} which has lightly damped poles. The nominal $\mathcal{H}_\infty$ controller has zeros at 389 Hz which is a dominant pole of G_{xx} which is also lightly damped. See Ref. [21] for a detailed description of these pole-zero cancellations in nominal $\mathcal{H}_\infty$ designs. Nominal $\mathcal{H}_\infty$ design without consideration for robustness is found to be inappropriate for the nanopositioner. Robust $\mathcal{H}_\infty$ designs which account for pole uncertainties is one way of tackling this problem at the expense of bandwidth.

Here it should be remarked that PI/PII controllers are not based on plant models and are designed to provide specific properties as high gains at low frequencies or asymptotic ramp signal tracking. On the other hand the $\mathcal{H}_\infty$ controllers are completely based on models - and therefore experimental results can deviate a lot from simulation predictions if inaccuracies in model are not adequately characterized. For instance, not including the pole-shift characterization lead to non robust implementation of $\mathcal{H}_\infty$ controllers.

Robust $\mathcal{H}_\infty$ design

In this design, The pole uncertainty in G_{xx} is characterized using multiplicative uncertainty. It can be shown that if a controller has to satisfy $\|w_p S\|_\infty \leq 1$ for plants belonging to a class $\mathcal{G}_{xx} = \{G_{xx}(1+w_i\Delta) : \|\Delta\|_\infty \leq 1\}$, then it is sufficient that, $\left\| \begin{matrix} w_p S \\ w_i T \end{matrix} \right\|_\infty \leq 1/\sqrt{2}$ is satisfied (see Ref. [20]). So in the original nominal $\mathcal{H}_\infty$ problem, the selection of $w_T = w_i$ fetches robust performance instead of just nominal performance. For G_{xx}, w_i was selected to be,

$$w_i(s) = \frac{0.84s^2 + 2214s + 5.3\times 10^6}{s^2 + 575.5s + 6.12\times 10^6}.$$

In the original $\mathcal{H}_\infty$ problem, w_T was chosen to be w_i to incorporate the added robust performance requirement. The resulting controller was 13th order given by,

$$K(s) = \frac{10617.6(s+1.5\times 10^4)(s+5818)(s+1717)(s+214.8)(s^2+1082s+5.17\times 10^6)}{s+1.85\times 10^4)(s+4.7)^2(s^2+2908s+3.88\times 10^6)(s^2+4167s+7.2\times 10^6)} \times \frac{(s^2+178.2s+6\times 10^6)(s^2+412.3s+1.6\times 10^7)(s^2+209.7s+5.616\times 10^7)}{(s^2+632.5s+9.3\times 10^6)(s^2+697.1s+4.53\times 10^7)(s^2+1.6\times 10^4 s+2\times 10^8)}$$

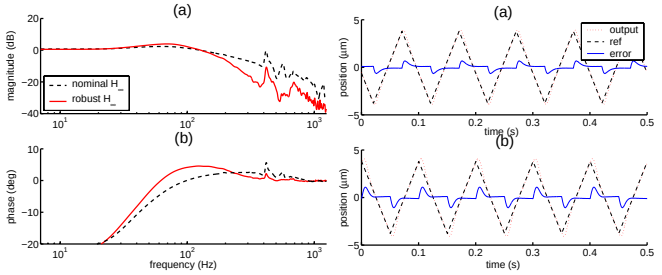

Figure 19. LEFT: THE SENSITIVITY AND COMPLEMENTARY SENSITIVITY FUNCTIONS ARE COMPARED FOR NOMINAL AND ROBUST $\mathcal{H}_\infty$ DESIGNS. RIGHT: a) TRACKING OF A 10HZ TRIANGULAR SIGNAL USING AN $\mathcal{H}_\infty$ CONTROLLER. b) TRACKING OF THE SAME SIGNAL USING A ROBUST $\mathcal{H}_\infty$ CONTROLLER.

The experimental plots are compared in Figure 19. It can be seen that the experimental closed loop transfer function plots have some features absent in the analytical plots. This is due to uncertainty in the plant model, particularly pole uncertainty. Figure 19 shows the experimental result of how the robust design introduces a dip in this frequency region thus reducing the magnitude of these unwanted peaks shows a 5 times reduction in the unwanted peak at near the dominant pole location due to the robust design). The right plot in the figure shows the tracking of 10 Hz triangular waves by nominal $\mathcal{H}_\infty$ and robust $\mathcal{H}_\infty$ controllers.

Glover-McFarlane control design

Here, we present the control design introduced by Glover and McFarlane (see Ref. [22] and Ref. [23]) which addresses *simultaneously* both the performance and robustness requirements. A remarkable feature of this design is that it achieves robustness with marginal reduction in performance. In fact, it is able to quantify the reduction by determining explicit bounds on how

much it changes the loop gains at low and high frequencies. This design process consists of two steps:

1. Design for performance: In this step, a shaping transfer function K_s is designed to meet the performance objectives of resolution and bandwidth (using corresponding loop shaping requirements on sensitivity and complementary sensitivity transfer functions). At this stage the requirements for robustness and even stability are not considered. In the design presented in this paper, K_s is set equal to PII controllers. This is done to retain the closed loop property of tracking ramp signals with zero steady state error.
2. Design of a robustifying controller: In this step, a robustifying controller K_r is obtained which gives good robustness properties to the closed loop system obtained from the shaped plant $G_s = K_s G_{xx}$ of the previous step.

The uncertainty is modelled as a combination of uncertainty in the numerator polynomial and the denominator polynomial of the nominal loop transfer function. More specifically if we represent the normalized coprime factorization of the nominal shaped plant by $G_s = \frac{N}{M}$, then the normalized coprime factor uncertainty characterization is given by,

$$\{\frac{N+\Delta_N}{M+\Delta_M} : \| \begin{bmatrix} \Delta_N & \Delta_M \end{bmatrix} \| \leq \varepsilon\},$$

In the second step of the design process, a controller is sought to stabilize the above set of plants. This characterization is very relevant to nanopositioning devices as it accounts for the plants with poles which are close to imaginary axis (as in the model of this device) and thus avoids control laws that "cancel" this poles. The robustness of the design is measured in terms of ε which is called the stability margin. Another attractive feature of this paradigm is the simplicity of the design procedure. The maximum stability margin can be computed $\varepsilon_{max} = (1+\rho(XZ))^{-1/2}$ a priori where ρ denotes the spectral radius, X and Z are the solutions of two algebraic Riccati equations (AREs). These AREs are completely determined by the state space realization of the nominal shaped system (see [20]). This a priori bound implies a simple one shot design of the controller (unlike the iterative process of $\mathcal{H}_\infty$ design) and directly characterizes the tolerable uncertainty.

As mentioned earlier an important feature of the Glover McFarlane design is that the loop transfer function before and after robustification is not significantly different. In fact in Ref. [23] it is shown that when $|G_s(j\omega)| > \sqrt{1/\varepsilon^2 - 1}$,

$$|K_r(j\omega)| \geq \frac{|G_s(j\omega)| - \sqrt{1/\varepsilon^2 - 1}}{\sqrt{1/\varepsilon^2 - 1}|G_s(j\omega)| + 1},$$

and when $|G_s(j\omega)| < 1/\sqrt{1/\varepsilon^2 - 1}$,

$$|K_r(j\omega)| \leq \frac{|G_s(j\omega)| + \sqrt{1/\varepsilon^2 - 1}}{1 - \sqrt{1/\varepsilon^2 - 1}|G_s(j\omega)|}.$$

The above inequalities show that in the frequency regions where $|G_s(j\omega)|$ is big and in the frequency regions where $|G_s(j\omega)|$ is small, there is a bound on the extent to which the robustifying controller changes the loop shape. If ε is large, then the changes to the loop shape in these frequency region is assured to be small.

Robustification of K_{pii}

The design process was applied to G_{xx} with K_s set to K_{pii} from previous subsection. A 9th order robustifying controller K_r was obtained which is given by,

$$K_r(s) = \frac{5227.6(s+5818)(s+31.45)(s^2+160.3s+5.98\times10^6)}{(s+2797)(s+5684)(s+294.8)(s^2+386.2s+6.6\times10^6)} \times \frac{(s^2+209.6s+5.6\times10^7)}{(s^2+397.3s+1.66\times10^7)(s^2+203.3s+5.62\times10^7)}.$$

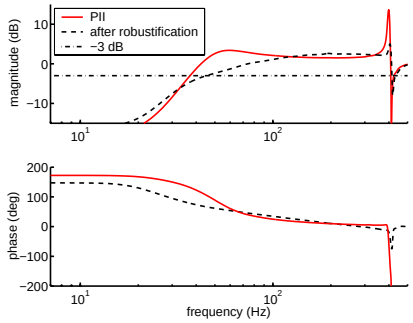

Figure 20. EXPERIMENTALLY OBTAINED $S(j\omega)$ OF K_{PII1} BEFORE AND AFTER ROBUSTIFICATION.

Figure 20 compares the experimentally obtained $S(j\omega)$ for K_{pii} before and after robustification. There is substantial reduction in the peak of $|S(j\omega)|$ due to the robustifying controller. The resulting lower bounds for GM and PM for the Glover McFarlane design is 2.3 and 33 degrees respectively which are significantly higher than 1.25 and 11.73 degrees for K_{pii}. Note that the bandwidth is comparable for both in spite of the significant difference in robustness.

More aggressive PII controllers can be implemented as the first step of the design does not impose stability requirements.

In Figure 21, the sensitivity function (experimental) of two such designs are shown. Designs 1 and 2 correspond to PII controllers $\frac{0.001s^2+600s+6\times10^5}{s^2}$ and $\frac{0.01s^2+500s+5\times10^5}{s^2}$ respectively. The PII controller in design 1 if used without robustification results in instability of the closed loop. However with robustification, these designs are stable and they guarantee good robustness margins with the added benefit of increased performance. The

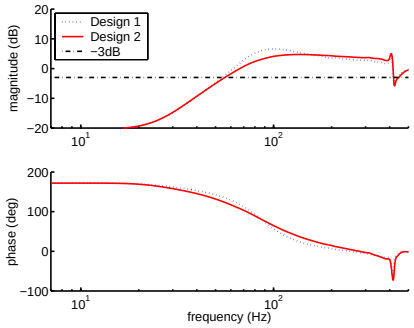

Figure 21. EXPERIMENTALLY OBTAINED SENSITIVITY FUNCTIONS OF THE GLOVER MCFARLANE DESIGNS

plots show significant increase in bandwidth ($> 55\ Hz$) without much loss in robustness (GM greater than 1.9 and PM greater than 29 degrees).

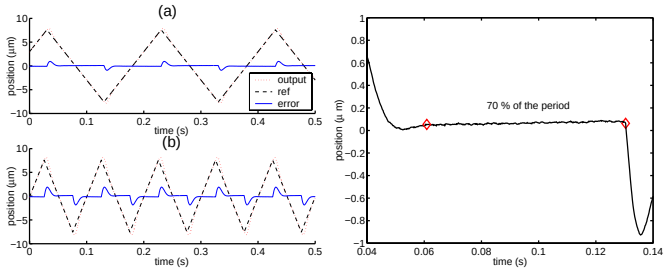

Figure 22. TRACKING OF 5 HZ AND 10 HZ TRIANGULAR SIGNALS USING A GLOVER MCFARLANE CONTROLLER. EXCEPT FOR THE TURN AROUND REGIONS, THE TRACKING IS VERY GOOD. FOR THE 5 HZ TRIANGULAR SIGNALS, ALMOST 70% OF THE PERIOD IS USABLE IN THIS CASE.

Triangular signals are tracked using the implemented Glover McFarlane designs. Figure 22 illustrates the tracking of 5 Hz and 10 Hz signals using the Glover McFarlane design 2. Except for the turn around points the tracking error is small. For the 5 Hz triangular signals, approximately 70% of the period is usable in this case compared to 30% for K_{pii} in spite of the larger amplitude of the reference waveform. Also these controllers are remarkably robust allowing the use of filters inside the loop to improve resolution. Since the performance and robustness requirements are decoupled, Glover McFarlane controllers can be used to robustify commonly used controllers like PII which have features like zero steady state error for ramp tracking. This is a significant advantage particularly when the nanopositioner is used for scanning applications.

Preview Based Control Design The designs presented above have the following features in common: 1) they are designed to obtain improvements in tracking (up to a bandwidth) of arbitrary reference signals, 2) they are based on causal feedback laws - the control signals do not depend on the future values of reference signals. However, in many applications, the reference signals are known in advance and therefore these signals can be used in designing anticipatory feedback laws to achieve better tracking performances. In particular, such advance knowledge of the reference trajectory can be used to achieve asymptotic perfect tracking of even those reference signals which have high frequency components. The primary advantages of preview control designs [24,25] are 1) addressing the limitations imposed by non minimum phase zeros - these limitations can be expressed as an upper limit on the bandwidth that may be achieved without necessarily incurring a large peak in the closed loop sensitivity function. In the case of preview control, the advance (anti causal) knowledge of the reference signal allows accurate rapid tracking over bandwidths which exceed normal performance limits. 2) to address the problem of requiring high gain actuator control laws. For minimum phase systems, high gain feedback laws (or employing infinite gains at tracking frequencies) usually achieve arbitrarily small tracking error signals. However, by using the feedforward terms in addition to feedback terms in preview control designs, asymptotic tracking can be achieved by having finite gains. Note that K_{ff} (Figure 23) represents a general linear operator which maps the complete reference signal $x_r(\cdot) = \{x_r(\tau)|\tau > 0\}$ to a current auxiliary control $u_d(t)$. This operator is not restricted to be proper or causal. The idea is to compute u_d such that $X_r(s) = G_{xx}(s)U_d(s)$ which requires the computation of $G_{xx}^{-1}(s)$. This computation presents two difficulties - the inverse may have negative relative degree and it can be unstable (when the plant is non minimum phase). These difficulties is resolved by decomposing u_d as

$$\begin{aligned} u_d &= u_0 + u_+ u_- \\ &= \sum_{i=1}^{l} q_l x_r^{(l)} + \left(\frac{R}{N_p}\right) \star x_r(\cdot) \\ &= \sum_{i=1}^{l} q_l x_r^{(l)} + \left(\frac{R^+}{N^+}\right) \star x_r(\cdot) + \left(\frac{R^-}{N^-}\right) \star x_r(\cdot) \end{aligned}$$

where l is the relative degree of G_{xx}, $\frac{R}{N_p}$ is a strictly transfer function, q_l are appropriate plant dependent parameters, N^+ (respectively N^-) has all zeros with positive (respectively negative) real parts. Thus u_- represents the usual stable (causal) implementation and u_+ represents the anti-causal implementation (see [24] for details) of the controller.

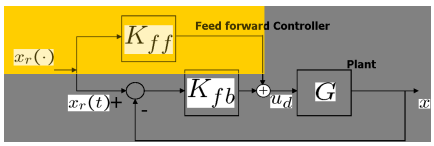

Figure 23. THE SYSTEM LOOP FOR PREVIEW CONTROL DESIGN.

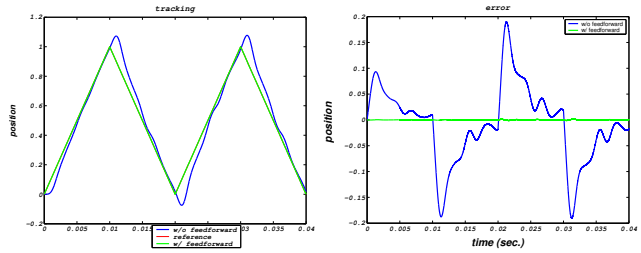

Figure 24. THE TRACKING OF A 50 HZ SIGNAL. THE TRACKING IS BAD WHEN THERE IS NO PREVIEW CONTROL (IN BLUE) AND THERE IS A SIGNIFICANT IMPROVEMENT WITH THE PREVIEW CONTROL (IN GREEN).

We employed this design methodology on the plant G_{xx} with K_{fb} being the PII feedback control law (design 2 presented in the Glover McFarlane design). Figure 24 shows the simulation results of this design implementation. We see that there is a great improvement in the tracking performance.

3.2.3 Characterization of the device

In this section the device is characterized in terms of static sensitivity, range, resolution, in the open and closed loop configurations. The Glover McFarlane design 2 described in section 3.2.2 is presented as an example.

Static sensitivity and travel range

The device was calibrated using a micro-cantilever and a 10 micron grating with 200 *nm* deep grooves. The grating is placed on the positioning stage and the micro-cantilever is brought in contact with the grating. The deflection of the cantilever and the LVDT sensor output are recorded as the stage is moved in the X direction. The range of the LVDT output was 16.27 V and the corresponding cantilever deflection showed the presence of 11 grooves which correspond to 110 μm. Hence the sensitivity of the X LVDT was found to be 6.76 $\mu m/V$.

Resolution

Since this device has no backlash (as there are no sliding parts) or any other such design restrictions, the resolution of the device is primarily determined by noise. However, this makes the comparison of resolution between the open and the closed loop configurations difficult. Theoretically, since in the closed loop designs, the noise is fed back to the actuator, they cannot achieve better resolutions than the open loop configurations. However,

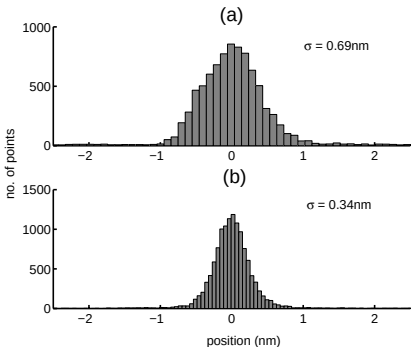

Figure 25. a) LVDT MEASUREMENT WITHOUT THE CONTROLLER. b) LVDT MEASUREMENT WHILE A CONTROLLER IS STABILIZING AT 0V.

the open loop devices are plagued by nonlinear effects such as drift and creep which make it very difficult to attain these theoretical values in a repeatable and predictable manner. On the other hand with these nonlinear effects being practically absent, the closed loop designs give much better access to accurate positioning. We emphasize here that though theoretically the open-loop resolutions are better (which may possibly be realized with very rigorous experiments and post data processing), it is much easier to predict and *realize* accurate positioning in the closed loop designs.

The resolutions can be characterized by associating appropriate metrics to the error signals $e_x = Tn$ if enough statistics describing n is available. This presents us the other problem we have with the characterization of the resolution. It is the fact that our measurements are limited by the resolution of the LVDT sensors, i.e., the device is capable of motions that are smaller

than which LVDT can detect. However, to get a quantitative feel of how small these error signals can be, the following experiment was done. The LVDT signals for both the open-loop and the closed-loop (Glover McFarlane) designs were measured when the system is at the nominal operating point. The measurement is taken over a small time window since in open loop the mean varies with drift, creep etc. Figure 25 shows that the variance of the sensor output while in open loop is higher than that in closed loop. This illustrates the improvement in 'resolution' due to feedback. It should be remembered that the closed loop resolution depends on the bandwidth and the shape of the corresponding complementary sensitivity functions. Better resolutions can be achieved by reducing the bandwidths.

4 Conclusions

We have presented the demands and challenges on nanopositioning devices. It has been shown that they fall naturally into the modern control theory paradigm. This theory provides an appropriate approach to quantify, incorporate and achieve *both* the performance and robustness objectives. Using this approach, we have obtained improvements of over sixty times in bandwidth and repeatable subnanometer resolution for these devices. The implementation of the Glover Mcfarlane design achieved substantial improvements in the robustness properties of previously designed PII controllers. One of the future goals is to design smaller positioning systems (to achieve higher bandwidths) and tackle the large "coupling" effects by designing appropriate MIMO controllers. The implementation of preview based control designs to obtain better tracking of a priori known reference signals is in progress.

Acknowledgements

This work was supported by NSF grant CMS-0201560 and the DARPA-UCLA sub-contract to Iowa State University under the MOSAIC initiative to Dr. Murti V. Salapaka. We would like to acknowledge the constant support of Dr. Murti Salapaka of Iowa State University and Dr. Jason Cleveland of *Asylum Research*. Thanks are also due to Todd Day, Dan Bocek, Dr. Mario Viani and the rest of *Asylum Research* for all the help during the course of the project.

REFERENCES

[1] Binnig, G., Quate, C., and Gerber, C., 1986. "Atomic Force Microscope". Physics Review Letters, **56** (9) [March], pp. 939–933.

[2] Crandall, B., 1996. *Nanotechnology: Molecular Speculation on Global Abundance*. MIT Press.

[3] Bhushan, B., 1995. *Handbook of Micro/Nano Tribology*. CRC Press.

[4] Crandall, B., 1996. *Nanotechnology: Molecular Speculation on Global Abundance*. MIT Press.

[5] Yves, M., 1995. *Scanning Probe Microscopes*. SPIE Press.

[6] White, D., and Wood, O., 2000. "Novel alignment system for imprint lithography". In Jurnal of Vacuum Science & Technology B (microelectronics and Nanometer structures), Rancho Mirage, vol. 18(6), pp. 3552–3556.

[7] Jianxu, M., and Ang Jr., M., 2000. "High-bandwidth macro/microactuation for hard disk drive". In Proceedings of the SPIE- the International Society for Optical Engineering, Boston, vol. 4194, pp. 94–102.

[8] Rihong, Z., X., D., Zhixing, Y., and Jinbang, C., 1998. "Research on systems for measurements of CCD parameters". In Proceedings of the SPIE- the International Society for Optical Engineering, vol. 3553, pp. 297–301.

[9] Krogmann, D., Tholl, H., Schreiber, P., Krehl, A., Goring, R., Gotz, B., and Martin, T., 1999. "Image multiplexing system on the base of piezoelectrically driven silicon microlens arrays". In 3^{rd} International Conference on Micro Opto Electro Mechanical Systems, MOEMS 99, Mainz, Germany., pp. 178–185.

[10] Meldrum, D., Pence, W., Moody, S., Cunningham, D., Holl, M., Wiktor, P., Saini, M., Moore, M., Jang, L.-S., Kidd, M., Fisher, C., and Cookson, A., 2001. "Automated, integrated modules for fluid handling, thermal cycling and purification of dna samples for high throughput sequencing and analysis.". In Proceedings of 2001 IEEE/ASME International conference on Advanced Intelligent Mekatronics, vol. 2, pp. 1211–1219.

[11] Whitesides, G., and Love, H., 2001. "The art of building small". Scientific American, **285** (3) [September], pp. 39–47.

[12] Barrett, R., and Quate, C., 1991. "Optical scan-correction system applied to atomic force microscopy". *Rev. of Sci. Instrum.*, **62** [], pp. 1393–1399.

[13] Koops, R., and Sawatzky, G., 1992. "New scanning device for scanning tunneling microscope applications". Review of Scientific Instruments, **63** (8) [August], pp. 4008–9.

[14] Kaizuka, H., 1989. "Application of capacitor insertion method to scanning tunneling microscopes". Rev. of Sci. Instrum., **60** (10) [], pp. 3119–3122.

[15] Croft, D., Shedd, G., and Devasia, S., 2000. "Creep, Hysteresis and Vibration compensation for Piezoactuators: Atomic Force Microscopy Application". In Proceedings of the American Control Conference, Chicago, Illinois, pp. 2123–2128.

[16] Daniele, A., Salapaka, S., Salapaka, M., and Dahleh, M., 1999. "Piezoelectric Scanners for Atomic Force Microscopes:Design of Lateral Sensors, Identification and Control". In Proceedings of the American Control Conference, San Diego, California, pp. 253–257.

[17] Schitter, G., Menold, P., Knapp, H. F., Allgower, F., and

Stemmer, A., 2001. “High performance feedback for fast scanning atomic force microscopes”. Review of Scientific Instruments, **72** (8) [August], pp. 3320–3327.

[18] Salapaka, S., Sebastian, A., Cleveland, J. P., and Salapaka, M. V., 2002. “High bandwidth nano-positioner: A robust control approach”. Review of Scientific Instruments, **73** (9) [September], pp. 3232–3241.

[19] Sebastian, A., and Salapaka, S., 2003. “$\langle_\infty$ loop shaping design for nano-positioning”. In Proceedings of the American Control Conference, Denver, Colorado, p. to appear.

[20] Skogestad, S., and Postlethwaite, I., 1997. *Multivariable Feedback Control, Analysis and Design*. John Wiley and Sons.

[21] Sefton, J., and Glover, K., 1990. “Pole/zero cancellations in the general $\mathcal{H}_\infty$ problem with reference to a two block design”. Systems and Control Letters, **14** (4) [].

[22] Glover, K., and McFarlane, D., 1989. “Robust stabilization of normalized coprime factor plant descriptions with $\mathcal{H}_\infty$-bounded uncertainty”. IEEE transactions on automatic control, **34** (8) [August], pp. 821–830.

[23] McFarlane, D., and Glover, K., 1992. “A loop shaping design procedure using $\mathcal{H}_\infty$ synthesis”. IEEE transactions on automatic control, **37** (6) [June], pp. 759–769.

[24] Chen, D., and Paden, B., 1996. “Stable inversion of nonlinear non-minimum phase systems”. International Journal of Control, **64** (1) [], pp. 81–97.

[25] Middleton, R., Freudenberg, J., and McClamroch, N., 2001. “Sensitivity and Robustness Properties in the Preview Control of Linear Non Minimum Phase Plants”. *Proceedings of the American Control Conference, Arlington, VA* [June], pp. 2957–62.